Radial macroscopic model of a plasma flowing along annular dielectric walls

E. Ahedo
E.T.S.I. Aeronáuticos, Universidad Politécnica de Madrid, 28040 Madrid, Spain

(Received 6 February 2002; accepted 15 April 2002)

The classical model of the transverse interaction of a collisionless, partially ionized plasma with two insulator walls confining it, is here generalized to plasmas flowing parallel to the walls. A macroscopic formulation is proposed, where the contributions of the axial flow are included into the radial equations through source terms for particle production, ion friction, and ion heating. These contributions compete with those due to ionization, and add three new parameters to the classical model. Zero-ionization cases are presented to show that the net production (and loss) of plasma can be independent of ionization. Friction effects on the radial ion acceleration is found to reduce plasma fluxes into the walls. The ion temperature is determined from the competition between heating due to ionization and cooling due to radial rarefaction; isothermal and isentropic behaviors are recovered only for particular situations. Planar and annular geometries are studied. For the latter one, the differences in the inner and outer plasma fluxes are evaluated. The application of the model to the plasma discharge in an annular Hall thruster is commented. © *2002 American Institute of Physics.* [DOI: 10.1063/1.1484157]

I. INTRODUCTION

The transverse interaction of a collisionless plasma with two dielectric walls confining it was treated originally by Tonks and Langmuir,[1] who solved the fundamental issues. The zero-current condition at the walls means that fluxes of ions and electrons to the walls must be equal, which implies a potential profile decreasing monotonically from around the center of the channel towards the two walls. Tonks and Langmuir showed that, in the zero Debye-length limit, the plasma structure consists of two thin non-neutral sheaths tied to the walls and a quasineutral region (the *presheath*) occupying the bulk of the channel. Each type of region is solved separately in their own distinguished scale. The condition for a correct presheath/sheath transition is *unique* and consists in the plasma flow being sonic there (the Bohm condition[2]). Apart from the three basic wall geometries, Tonks and Langmuir (interested in thin cylindrical probes immersed in cylindrical channels) discussed the case of an annular geometry, pointing out the lack of symmetry between the profiles of the inner and outer presheaths (these ones separated by the point of maximum electric potential).

A central contribution of Tonks and Langmuir is the *plasma balance equation*, which establishes the plasma production rate required to sustain a steady-state discharge. This production rate is proportional to the channel width, as it comes out from equating the volumetric production of plasma to the losses at the walls. In Tonks–Langmuir model, where plasma production is dominated by ionization, the plasma balance equation fixes the ionization rate and, as a consequence, the plasma temperature; indeed, a steady-state discharge is not possible when the plasma production rate is larger than the maximum ionization rate of the gas. Tonks and Langmuir considered different radial profiles for the ionization rate, but it was shown later that the mean value of the plasma production rate is independent of its radial profile.[3,4]

Bissell *et al.*[5] (reviewing several other papers) and Scheuer and Emmert[6] propose macroscopic formulations of the Tonks–Langmuir problem (for planar geometry only), with different closure hypotheses for the ion energy equation. They conclude that macroscopic models can approximate well the kinetic results, mainly in relation to particle and energy fluxes towards the walls.

As the Tonks–Langmuir model, these fluid models include ionization as the only source term in the plasma equations and, therefore, are restricted to no-flowing plasmas basically. When there is plasma flow parallel to the walls, the problem becomes two dimensional (2D), with mutual interaction between the longitudinal and transverse (i.e., axial and radial) dynamics. However, at each axial cross section (of a long channel) we may consider the one-dimensional (1D) problem that describes the radial dynamics of the plasma. This requires to take into account the influence of the axial flow on the radial motion. In the macroscopic formulation this can be modeled with adequate source terms in the radial equations.

The goal of this paper is to generalize the presheath/sheath model of Tonks–Langmuir to plasmas flowing axially, with emphasis on the coupled influence of ionization and axial flow on the radial solution. In a preliminary study (with planar geometry and cold ions) we showed already that losses to the wall are reduced by an effective radial friction due to axial variations of the radial conditions.[7] Here we develop the general model for warm ions and annular geometries. Thus, planar, cylindrical, and annular channels are covered; the differences between the inner and outer presheaths in the latter case are an extra aspect of interest. No secondary emission at the walls will be considered here, so that the sheath problem reduces to a well-known solution

and the attention of the paper is focused on the presheath model.

An application of the present work is the plasma discharge in an annular Hall thruster. Since an accurate two-dimensional analysis of this problem is unavailable yet, partial analyses of the radial and axial problems are of great interest. In particular, the knowledge of the radial plasma structure would allow one to estimate the losses at the lateral walls at each cross section, which could then be included as sink terms in 1D axial models of the discharge.[8,9] The 2D Hall thruster discharge has been chosen here as the basis to formulate the 1D radial model for a flowing plasma. However, we believe this radial model to be general enough to apply to other flowing plasmas interacting with two walls. In order to emphasize this and to free the radial model from the Hall thruster case, the derivation of the 1D radial model from the 2D axisymmetric model of the discharge has been confined to Appendix A.

In a recent paper on a 2D model of the Hall thruster, Keidar *et al.* use a presheath/sheath model for the lateral walls.[10] They claim that for a smooth presheath/sheath solution the radial ion velocity at the sheath transition must be *smaller* than the (sonic) Bohm velocity, in contradiction to the well established sheath theory between a wall and a plasma.[1,11] The main arguments supporting the sonic velocity as the correct transition condition are recalled in Appendix B. Comments on other aspects of Keidar's paper, like their results on the interaction between the axial and radial responses are out of the scope of this paper.

The rest of the paper is organized as follows. In Sec. II we formulate the radial model, the boundary and compatibility conditions, and the integration procedure. In Sec. III we discuss solutions for different cases and geometries. Conclusions are presented in Sec. IV.

II. MODEL FORMULATION

A. The quasineutral presheath

Figure 1 sketches the situation on an axial cross section of an annular chamber. The plasma is supposed to flow axially between two long dielectric walls placed, in cylindrical coordinates (x,r,θ), at $r=r_{W'}$ and $r=r_W=r_{W'}+h$, with h the channel width. We consider the zero Debye-length limit, $\lambda_d/h\to 0$, allowing a two-scale, presheath/sheath analysis with h and λ_d the distinguished scales of presheath and sheaths, respectively. From Appendix A, the pertinent 1D fluid equations in the presheath are

$$\frac{1}{r}\frac{\partial}{\partial r} r n_i v_{ri} = \nu_w n_i , \tag{1}$$

$$m_i n_i v_{ri}\frac{\partial v_{ri}}{\partial r} = -\frac{\partial}{\partial r}(n_i T_i) - e n_i \frac{\partial \phi}{\partial r} - \nu_r m_i n_i v_{ri} , \tag{2}$$

$$\frac{1}{r}\frac{\partial}{\partial r}\left(r\frac{3}{2} T_i n_i v_{ri}\right) + \frac{T_i n_i}{r}\frac{\partial}{\partial r}(r v_{ri}) = \nu_i \tfrac{1}{2} m_i n_i v_{ri}^2 + \nu_t n_i T_i , \tag{3}$$

$$n_e = \text{const}\times \exp(e\phi/T_e), \tag{4}$$

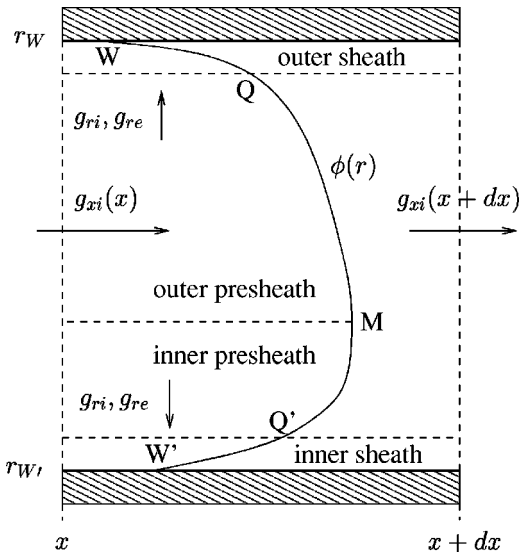

FIG. 1. A generic radial section of a long annular channel between two dielectric walls. $g_{xi}=n_{xi}v_{xi}$ and $g_{ri}=n_{ri}v_{ri}$ represent axial and radial particle fluxes; $\phi(r)$ sketches the radial profile of the electric potential, which is maximum at point M. The transitions to the sheaths are at points Q and Q'. Since the presheath/sheath structure corresponds to the zero Debye-length limit one has $r_W=r_Q$ and $r'_W=r'_Q$.

$$n_e = n_i . \tag{5}$$

Here ν_i, ν_w, ν_r, ν_t are frequencies for ionization, ion net production, effective radial friction, and axial energy contribution, respectively, defined in Eq. (A8). We assume these frequencies to be known functions of r in any axial position. Moreover, we restrict the discussion here to $\nu_j(r)=\text{const}$ $(j=i,w,r,t)$, because there are no fundamental novelties when treating more general profiles (see Ref. 4 and comments in Sec. III A).

Operating with the above equations, the radial problem in the presheath reduces to integrate the two coupled equations

$$\left(T_e + \frac{5}{3} T_i - m_i v_{ri}^2\right)\frac{\partial v_{ri}}{\partial r} = \left(\nu_r + \frac{\nu_i}{3}\right) m_i v_{ri}^2 - \left(T_e + \frac{5}{3} T_i\right)\frac{v_{ri}}{r} + \nu_w\left(T_e + \frac{5}{3} T_i\right) + (\tfrac{2}{3}\nu_t - \tfrac{5}{3}\nu_w) T_i , \tag{6}$$

$$\frac{3}{2} v_{ri}\frac{\partial T_i}{\partial r} = \nu_i \frac{1}{2} m_i v_{ri}^2 - T_i\left(\frac{\partial v_{ri}}{\partial r} + \frac{v_{ri}}{r}\right) + \nu_w T_i + (\nu_t - \tfrac{5}{2}\nu_w) T_i , \tag{7}$$

plus one differential equation for the electric potential,

$$v_{ri}\frac{\partial}{\partial r}\left(\frac{e\phi}{T_e}\right) = \nu_w - \frac{1}{r}\frac{\partial}{\partial r}(r v_{ri}), \tag{8}$$

which corresponds to the so-called *plasma equation* in kinetic models.[1]

Equation (6) shows that radial derivatives become singular at

$$|v_{ri}| = c_s(T_i) \equiv \sqrt{\frac{T_e + \frac{5}{3}T_i}{m_i}}, \tag{9}$$

with c_s the local sound velocity of the plasma. In particular, the electric field, $d\phi/dr$, becomes infinite there, indicating the failure of the quasineutral approximation and the transition from the large h scale to the thin λ_d scale of the sheath. Therefore,

$$v_{riQ} = c_{sQ}, \quad v_{riQ'} = -c_{sQ'}, \tag{10}$$

are the Bohm conditions defining the transition points (Q and Q' in Fig. 1) to the outer and inner non-neutral sheaths. In Appendix B we show that these transition conditions are the only valid ones.

The electric potential must present a maximum at some intermediate position of the channel (point M in Fig. 1), $\partial\phi/\partial r|_M = 0$. A local expansion of Eqs. (6)–(8) around point M yields

$$\begin{aligned} v_{ri}(r) &= \nu_w(r - r_M) + O[(r - r_M)^2], \\ T_i(r) &= T_{iM} + O[(r - r_M)^2], \end{aligned} \tag{11}$$

and the compatibility condition

$$\nu_t = 5\nu_w/2. \tag{12}$$

As Eq. (A10) in Appendix A confirms, this condition corresponds to the correct balance between the radial and axial fluxes of the ion internal energy.

Condition (12) makes identically zero the last term of each of the equations (6) and (7). Then, for the zero-ionization case ($\nu_i = 0$), Eqs. (1) and (3) yield the isentropic law

$$\frac{T_i}{n_i^{2/3}} = \text{const}, \tag{13}$$

which substitutes to Eq. (7).

Convenient dimensionless variables to integrate Eqs. (6)–(8) are

$$\begin{aligned} &\tilde{r} = \frac{r}{h}, \quad \tilde{T}_i = \frac{T_i}{T_e}, \quad \tilde{\phi} = \frac{e(\phi - \phi_M)}{T_e}, \\ &\tilde{v}_{ri} = \frac{v_{ri}}{\sqrt{T_e/m_i}}, \quad \tilde{\nu}_j = \frac{\nu_j}{\nu_0} \quad (j = i, w, r, t), \end{aligned} \tag{14}$$

with

$$\nu_0 = h^{-1}\sqrt{T_e/m_i} \tag{15}$$

the characteristic frequency for radial processes. The convenient integration procedure departs from point M towards points Q and Q', using the expansions of Eq. (11) as initial conditions. The two independent integrations end where Bohm conditions (10) are satisfied, and determine $\tilde{r}_Q$ and $\tilde{r}_{Q'}$ in terms of five input parameters: $\tilde{T}_{iM}$, $\tilde{r}_M$, $\tilde{\nu}_i$, $\tilde{\nu}_r$, and $\tilde{\nu}_w$, while $\tilde{\nu}_t$ satisfies Eq. (12).

The sheaths thicknesses are of the order of the Debye length. Thus, in the zero Debye-length limit, the sheaths are seen as two plasma discontinuities in the presheath scale

$$r_W \simeq r_Q, \quad r_{W'} \simeq r_{Q'}. \tag{16}$$

Since the channel width is known, the presheath solution must satisfy the condition

$$\tilde{r}_Q - \tilde{r}_{Q'} = 1.$$

This implies an extra relation among the above five input parameters. After exchanging $\tilde{r}_M$ by the annular ratio

$$\beta = r_{W'}/r_W,$$

as known parameter, the extra relation leads to a relationship

$$\tilde{\nu}_w = \tilde{\nu}_w(\tilde{\nu}_i, \tilde{\nu}_r, \tilde{T}_{iM}, \beta). \tag{17}$$

This is the generalized form of the Tonks–Langmuir plasma balance equation for flowing plasmas and annular geometries; the limits $\beta \to 1$ and $\beta = 0$ correspond to the planar and cylindrical cases, respectively.

The comparison of the present model, Eqs. (1)–(5), with those of Refs. 5 and 6, shows that these ones cover only the cases (i) $\beta = 1$ (i.e., a planar geometry) and (ii) $\nu_r = \nu_i = \nu_w$ (i.e., a no flowing plasma). Therefore, the four free parameters of Eq. (17) are reduced in their case to just one, $\tilde{T}_{iM}$. Also, these no-flowing models use $\nu_i \frac{3}{2} T_n$ in Eq. (3) instead of $\nu_t T_i$, which agrees with Eq. (A8) for the no-flowing case. This difference in the heating term has interesting consequences on the balance/compatibility condition for the internal energy. In our model, the term $\nu_t T_i$ leads to the compatibility condition (12), which states that the radial heating frequency, ν_t, depends on the radial production/loss frequency, ν_w, whereas the value of T_{iM} is *free* (which agrees with the idea of T_{iM} depending partially on the axial discharge conditions). On the contrary, in the no-flowing models of Refs. 5 and 6, which do not include the heating frequency ν_t (that is, they neglect any axial contribution to ion heating), the balance/compatibility condition *fixes* the value of T_{iM} (as proportional to T_n). (Differences in the definitions of the ion temperature in the different models have no relevant consequences and have then been ignored in the preceding discussion.)

B. The sheaths

The role of the two radial sheaths, $W'Q$ and QW in Fig. 1, is to provide the potential drop needed to maintain the zero-current condition at the wall. For the zero Debye-length limit, the sheaths are collisionless boundary layers perpendicular to the walls. The 2D Poisson equation, Eq. (A12), reduces to the 1D radial form, Eq. (B1), and plasma equations (1)–(5) become algebraic, conservation relations for the fluxes of different plasma magnitudes. In particular and taking the case of the outer sheath, the ion density flux to the outer wall, $g_{riW} = (n_i v_{ri})_W$, satisfies

$$g_{riW} = g_{riQ} = n_{iQ} c_{sQ}, \tag{18}$$

with $n_{iQ} = n_{iM} \exp(-e\phi_{QM}/T_e)$ and $\phi_{QM} = \phi_M - \phi_Q$ the potential drop at the presheath.

For no secondary emission at the walls and a semi-Maxwellian distribution of the electrons, the zero current condition follows:

$$g_{riQ}=n_{eQ}\exp\left(-\frac{e\phi_{WQ}}{T_e}\right)\sqrt{\frac{T_e}{2\pi m_e}}, \tag{19}$$

with $\phi_{WQ}=\phi_Q-\phi_W$ the potential drop at the sheath. Solving for ϕ_{WQ}, one has

$$\frac{e\phi_{WQ}}{T_e}=\frac{1}{2}\left[\ln\frac{m_i}{2\pi m_e}-\ln\left(1+\frac{5T_{iQ}}{3T_e}\right)\right]. \tag{20}$$

For all practical values of T_{iQ}/T_e, the last term on the right-hand side can be disregarded, so that the sheath potential drop is practically independent of the presheath solution.

The above expressions relate the main sheath parameters. The Poisson equation (B1) needs to be solved only to determine the spatial structure of the sheath and to find, in a way equivalent to that used in Appendix B, that the (outer) sheath solution exists only for $v_{riQ}\geqslant c_{sQ}$.

III. PLANAR AND ANNULAR SOLUTIONS

A. Planar geometry: Cold ions

We consider first the simple case

$$\beta\to 1,\quad \tilde{T}_{iM}=0,\quad \tilde{\nu}_i\to 0. \tag{21}$$

The first condition implies that the channel is quasiplanar (satisfying $1/r\ll\partial/\partial r$), so that the presheath is composed by two symmetric regions, with $r_M=(r_Q+r_{Q'})/2$ the channel midpoint, and we just need to solve the region MQ. The second and third conditions yield $\tilde{T}_i(r)=\text{const}=0$ as the solution of Eq. (7).

For the basic no-friction case, $\tilde{\nu}_r=0$, the velocity and potential profiles [Eqs. (6) and (8)] satisfy

$$\tilde{v}_{ri}-\tilde{v}_{ri}^3/3=(\tilde{r}-\tilde{r}_M)\tilde{\nu}_w,\quad \tilde{\phi}=-\tilde{v}_{ri}^2/2. \tag{22}$$

Setting $\tilde{v}_{riQ}=1$ at $\tilde{r}_Q=\tilde{r}_M+1/2$ [Eq. (10)] one has

$$\tilde{\nu}_w=4/3, \tag{23}$$

which is the plasma balance condition for this basic case. It states that the total production frequency is fixed by the channel width and the plasma temperature. Notice that the plasma balance condition is the consequence of two facts: (a) wall electrical properties imply the presence of a thin non-neutral sheath; and (b) the transition to this sheath requires the ion flow to be sonic.

[Were not the frequency profile $\nu_w(r)$ constant, $(\tilde{r}-\tilde{r}_M)\tilde{\nu}_w$ in Eq. (22) should be substituted by $\int_{\tilde{r}_M}^{\tilde{r}}\tilde{\nu}_w(\tilde{r}')d\tilde{r}'$, and the balance condition would yield $\int_{\tilde{r}_{W'}}^{\tilde{r}_W}\tilde{\nu}_w(\tilde{r}')d\tilde{r}'=4/3$. Since v_{ri} must be zero at point M and equal to $\pm c_s$ at the walls, the shape of $\nu_w(r)$ modifies only the local gradients of $v_{ri}(r)$: when ν_w tends to concentrate around point M, v_{ri} tends to present an intermediate inflexion point.[4] In any case, since the shape of $\nu_w(r)$ depends on both the axial flux and the ionization rate, very steep shapes are unlike.]

For the positive friction case $\tilde{\nu}_r>0$, Eqs. (6) and (8) yield

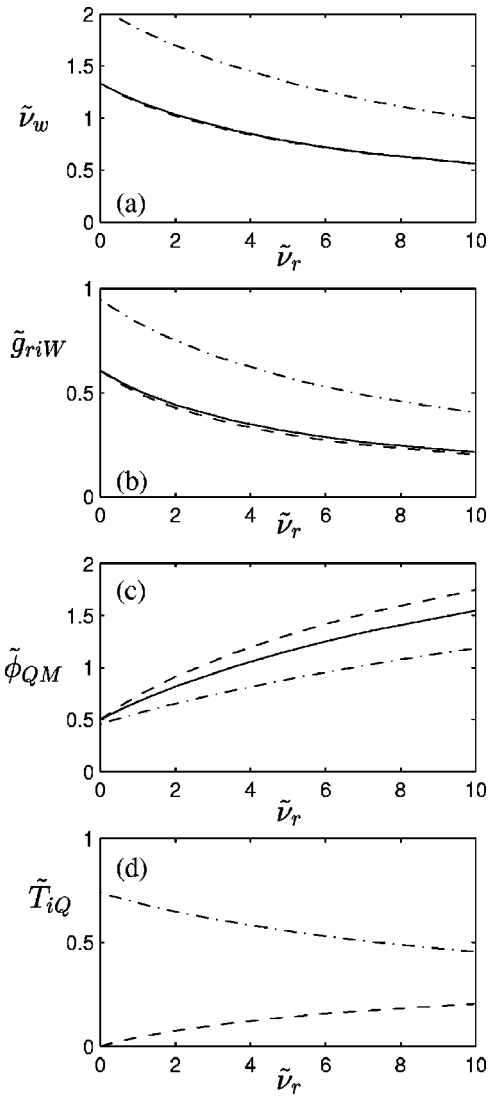

FIG. 2. Planar geometry: Evolution of plasma parameters with $\tilde{\nu}_r$ for $(\tilde{T}_{iM},\tilde{\nu}_i)=(0,0)$ [solid line], (1,0) [dashed–dotted line], and $(0,\tilde{\nu}_r)$ [dashed line]. The dimensionless particle flux is $\tilde{g}_{ri}=(n_{iM}\sqrt{T_e/m_i})^{-1}g_{ri}$.

$$\frac{1+\alpha_r}{\sqrt{\alpha_r}}\arctan(\tilde{v}_{ri}\sqrt{\alpha_r})-\tilde{v}_{ri}=\alpha_r\tilde{\nu}_w(\tilde{r}-\tilde{r}_M), \tag{24}$$

$$\tilde{\phi}=-\frac{1+\alpha_r}{2\alpha_r}\ln(1+\alpha_r\tilde{v}_{ri}^2), \tag{25}$$

with $\alpha_r=\nu_r/\nu_w$ a convenient parameter.[7] Setting $\tilde{v}_{riQ}=1$ at $\tilde{r}=\tilde{r}_M+1/2$, one obtains the plasma balance condition relating now $\tilde{\nu}_w$ to $\tilde{\nu}_r$. Figures 2(a)–2(c) (case $\tilde{T}_{iM}=0$ and $\tilde{\nu}_i=0$) show the evolution of the production frequency, the potential drop at the presheath, and the plasma current to the wall with the friction frequency. For $\tilde{\nu}_r\to 0$, one recovers $\tilde{\nu}_w=4/3$ and $\tilde{\phi}_{QM}=1/2$; for $\tilde{\nu}_r\gg 1$, one has $\tilde{\nu}_w\simeq\pi^2/\tilde{\nu}_r$ and $\tilde{\phi}_{QM}\simeq\ln\tilde{\nu}_r$. These results indicate that larger ion frictions (i) mean larger potential and density drops across the channel in order to bring the ion flow to the sonic condition, $\tilde{v}_{riQ}=1$, at the sheath tied to the wall, and (ii) yield lower production frequencies. Therefore, the axial motion turns out to be an efficient mechanism to inhibit the plasma losses to the wall.

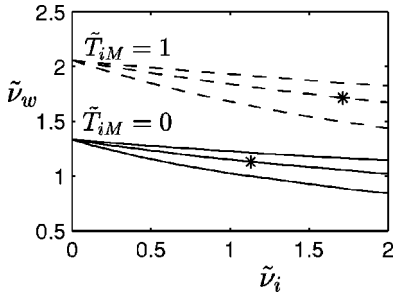

FIG. 3. Planar geometry: Net production frequency versus ionization frequency for $\tilde{T}_{iM}=0$ (solid lines) and 1 (dashed lines) and $\nu_i/\nu_r=0.5$, 1, and 2 (from bottom to top for each $\tilde{T}_{iM}$). The asterisks correspond to the no-flowing case, $\nu_w=\nu_i=\nu_r$.

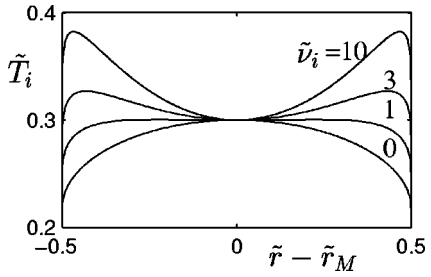

FIG. 4. Planar geometry: Radial profiles of the ion temperature for $\tilde{T}_{iM}=0.3$, $\tilde{\nu}_r=\tilde{\nu}_i$, and four ionization frequencies: $\tilde{\nu}_i=0$, 1, 3, and 10.

However, the ion axial motion can lead to negative values of $\tilde{\nu}_r$ too, which increase the plasma current to the wall. For $\tilde{\nu}_r<0$, $\tilde{v}_{ri}(\tilde{r},\tilde{\nu}_r)$ and $\tilde{\nu}_w(\tilde{\nu}_r)$ satisfy

$$\tilde{v}_{ri}+\frac{1+\alpha_r}{2|\alpha_r|^{1/2}}\ln\frac{1-\tilde{v}_{ri}|\alpha_r|^{1/2}}{1+\tilde{v}_{ri}|\alpha_r|^{1/2}}=|\alpha_r|\tilde{\nu}_w(\tilde{r}-\tilde{r}_M), \tag{26}$$

and Eq. (10). These relations show that $\partial\nu_w/\partial(-\nu_r)>0$, but solutions with negative friction exist only up to $\tilde{\nu}_r=-2$ (yielding $\tilde{\nu}_w=2$). Were $-\tilde{\nu}_r>2$, the plasma velocity would not reach the Bohm velocity, Eq. (10), and a steady radial solution would not form.

B. Planar geometry: General solution

To solve numerically Eqs. (6)–(8) for $\tilde{\nu}_i>0$, $\tilde{T}_{iM}>0$, and $\beta=1$, we use the spatial variable $\xi=\tilde{\nu}_w(\tilde{r}-\tilde{r}_M)$ and the ratios $\alpha_j=\nu_j/\nu_w$ $(j=r,i)$. The integration from points M to Q yields the relation $\tilde{\nu}_w=2\ \xi_Q(\alpha_r,\alpha_i,\tilde{T}_{iM})$, where from the plasma balance condition $\tilde{\nu}_w=\tilde{\nu}_w(\tilde{\nu}_r,\tilde{\nu}_i,\tilde{T}_{iM})$ is obtained.

The comparison of the solid and dashed–dotted lines in Figs. 2(a)–2(d) illustrates the effect of warm ions on zero-ionization situations. First, since the plasma sound speed increases with $\tilde{T}_{iM}$, one has that $\tilde{\nu}_w$ and wall losses increase too. Second, for $\tilde{\nu}_i=0$, $T_i(r)$ decreases towards the walls following the isentropic law (13) and yielding

$$T_{iQ}/T_{iM}=\exp(-3\tilde{\phi}_{QM}/2)<1.$$

Figure 3 and the dashed line of Figs. 2(a)–2(d) illustrate the influence of $\tilde{\nu}_i$ for different values of $\tilde{\nu}_i/\tilde{\nu}_r$. Although $\tilde{\nu}_i$ contributes to ν_r [Eq. (A8)], for the present discussion it is convenient to take them as independent parameters. Then, Figs. 2(a) and 2(b) indicate that $\tilde{\nu}_r$, and not $\tilde{\nu}_i$, determine the net production frequency. The main effect of $\tilde{\nu}_i$ is to increase the dispersion of ion velocities, that is the ion temperature. Figure 4 shows the competition between the cooling effect of ion rarefaction [Eq. (13)] and the ion heating due to ionization.

The no axial-flow case, $\tilde{\nu}_w=\tilde{\nu}_r=\tilde{\nu}_i$, treated by Tonks and Langmuir and Refs. 5 and 6, corresponds to a *single* solution point for each $\tilde{T}_{iM}$; these are the asterisks marked in Fig. 3. As Tonks and Langmuir explained (for $\tilde{T}_{iM}=0$), the plasma balance condition in the no axial-flow case determines totally the ionization frequency, ν_i, and, therefore, the electron temperature. In cases where the axial flow is relevant (like the plasma discharge in a Hall thruster), T_e is determined by the axial energy balance mainly,[12] and the difference between $\nu_i(T_e)$ and the total production frequency, $\nu_w(T_e,h)$ is provided by the axial variation of the ion axial flux [Eq. (A9)]. Finally, notice that in the Tonks–Langmuir problem, a steady-state plasma discharge requires ν_w to be less than the absolute maximum of $\nu_i(T_e)$, whereas in a plasma flowing axially, the steady-state solution relies more on axial conditions.

C. Annular geometry

In this general case the convenient integration variable of Eqs. (6)–(8) is $\eta=\tilde{r}\tilde{\nu}_w$. The separate integrations of the presheath equations from point M towards points Q and Q', which includes η_M as an input parameter, yields $\eta_{Q'}$ and η_Q as functions of η_M, α_r, α_i, and $\tilde{T}_{iM}$. Then, using the two equalities

$$\tilde{\nu}_w=\eta_Q-\eta_{Q'}=\eta_Q/\tilde{r}_Q, \tag{27}$$

the plasma balance condition in the form of Eq. (17) is obtained.

Figures 5(a)–5(c) depict spatial profiles of different magnitudes for zero-ionization cases ($\nu_i=0$) and different annular ratios. Point M tends to drift towards the inner wall as β decreases, yielding two asymmetric presheaths, with steeper gradients in the inner one, as Tonks and Langmuir deduced. Plasma gradients tend to diverge as $\beta\to 0$, but the solution cannot be continued down to $\beta=0$ (i.e., a cylindrical chamber), since then point M coincides with the channel axis and the inner presheath disappears.

For $\nu_i=0$, the ion temperature follows the isentropic law (13). Consequences of this and the Bohm conditions (10), are $v_{riQ}=v_{riQ'}$ and $n_{iQ}=n_{iQ'}$, independently of β. Therefore, in spite of the presheath asymmetry, one has equal wall currents and potential drops in both presheaths,

$$\nu_i=0:\quad g_{riW}=g_{riW'},\quad \phi_{Q'M}=\phi_{QM}.$$

Figures 6(a)–6(c) show, for different β, the evolution with $\tilde{\nu}_i$ of the main parameters of the inner and outer presheaths. In Fig. 6(a) we see that $\tilde{\nu}_w$ is affected weakly by β; notice that, similar to Fig. 3, the no axial-motion case corresponds to just one point: $\tilde{\nu}_w=\tilde{\nu}_i$, for each β line. Figures 6(b) and 6(c) show that for $\tilde{\nu}_i>0$ and $\beta<1$, wall currents and potential drops are different in the two presheaths.

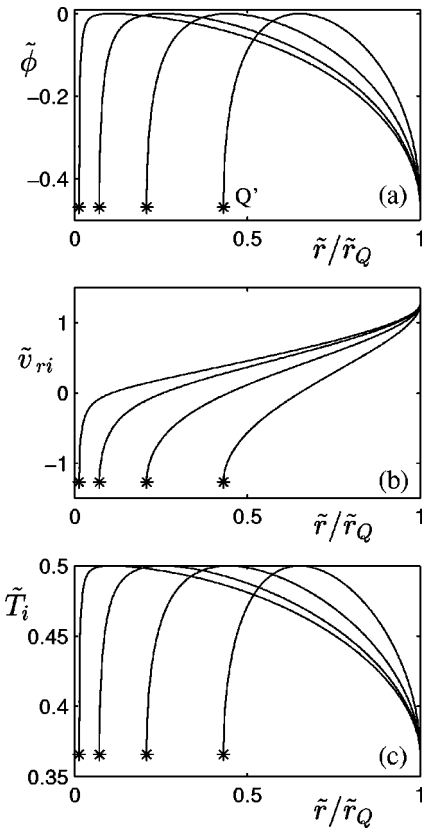

FIG. 5. Annular geometry: Plasma profiles for different annular ratios ($r'_Q/r_Q \simeq 0.013, 0.072, 0.21, 0.43$), $\tilde{T}_{iM}=0.5$, and $\tilde{\nu}_r=\tilde{\nu}_i=0$. Points Q' are at the asterisks; points M are at $d\phi/dr|_M=0$ (and $\tilde{v}_{ri}=0$) separating the inner and outer presheaths.

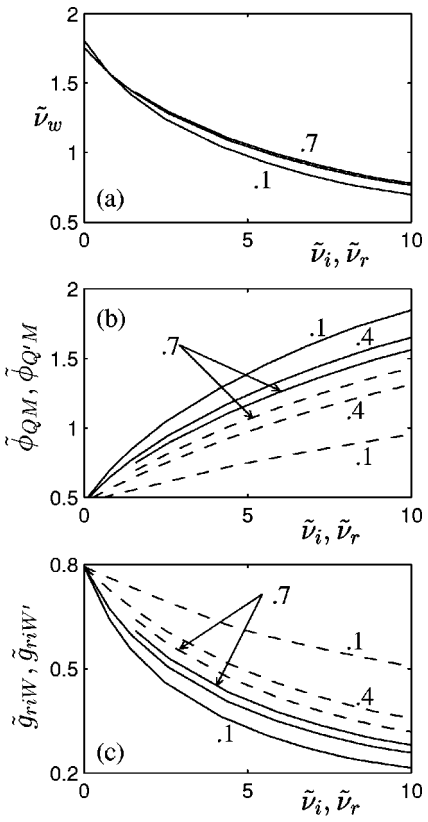

FIG. 6. Annular geometry: Evolution of main plasma parameters with $\tilde{\nu}_i$ for $\tilde{T}_{iM}=0.5$, $\tilde{\nu}_r=\tilde{\nu}_i$ and three annular ratios, $\beta=0.1$, 0.4, and 0.7. In (b) and (c) solid lines correspond to the outer presheath, and dashed lines to the inner presheath.

Differences increase as β decreases; departures from the planar solution become relevant for $\beta<0.7$, roughly. Taking as a reference the planar case, potential drops tend to be smaller in the inner presheath and larger in the outer one [Fig. 6(b)] whereas plasma currents [Fig. 6(c)] follow the opposite behavior. The sheath solution (20) indicates that presheath asymmetries of an annular chamber do not produce further asymmetries in the inner and outer sheaths. In conclusion, in an annular chamber with nonzero ionization the particle and energy fluxes are larger at the inner wall than at the outer one.

Ion temperatures at points Q and Q' for the cases of Fig. 6 are about $0.4-0.5T_e$ and their dependence on $\tilde{\nu}_r$ and β follow the trends of the respective potential drops. For $\tilde{\nu}_i=0$, $\tilde{\nu}_r>0$, and the rest of conditions the same as in Fig. 6, results are very similar to those of Fig. 6, except for the ion temperatures, which are smaller due to the isentropic behavior, Eq. (13).

IV. SUMMARY

A model of the radial structure of a plasma flowing along two dielectric walls must take into account the contributions of the axial flow into the radial equations. In a macroscopic formulation, this can be done by including three terms, representing a particle source, an effective friction, and an internal energy source in the equations of continuity, momentum, and energy, respectively. The production/loss of ions may come from either ionization or the axial flow; the effective radial friction comes from both ionization and the axial variation of the radial velocity; and the internal energy of the axial flow contributes to the energy balance. Compared to the classical model of Tonks–Langmuir (and its macroscopic versions) the present model has three new parameters (or degrees of freedom): a net ion production/loss frequency, ν_w (which is independent of the ionization frequency, ν_i), a frequency for ion radial friction, ν_r, and the ion temperature, T_{iM}, at the point separating inner and outer radial flows.

The plasma balance condition of Tonks–Langmuir stated that geometrical magnitudes determined ν_i and, as a result, the electron temperature. In the present model, the plasma balance condition yields ν_w as a function of the effective radial friction, the ionization rate, the temperature T_{iM}, and geometrical magnitudes, whereas T_e remains a free parameter (to be determined from the axial conditions of the discharge). The investigation of the plasma balance condition reveals two important conclusions. First, ν_w depends significantly on ν_r in a way such that a strong radial friction can reduce significantly the loss of plasma current into the lateral walls. And second, ν_i has practically no direct influence on ν_w; the indirect influence comes from the contribution of ν_i to ν_r.

The equation for the ion internal energy includes two source terms: one due to the velocity dispersion of the ion

fluid because of ionization, and the second one coming from the mean temperature of the ion sources (ionization and axial flow). As a consequence, T_{iM} is partially independent of the temperature of the neutral gas, T_n. Regarding the thermodynamic response of the ions, it is shown that (i) an isothermal behavior exists only for the zero-ionization and zero-temperature limit; (ii) an isentropic response takes place for zero-ionization, with radial rarefaction producing ion cooling; and (iii) for $\nu_i>0$ and $T_{iM}>0$, heating due to ionization competes with the rarefaction cooling in shaping the ion temperature profile.

The analysis of channels with different annular ratios, shows that asymmetries between the profiles of the inner and outer presheaths are relevant for $\beta<0.7$, roughly. Point M of maximum potential moves towards the inner wall as β decreases, and plasma gradients are larger in the inner presheath. In spite of that presheath asymmetry, for $\nu_i=0$ the potential drops and the currents into the walls are the same in the inner and outer presheath. For $\nu_i \geqslant O(1)$, smaller potential drops and larger wall currents are found in the inner presheath. Plasma currents remain constant inside the sheaths and the sheath potential drops are practically independent of the presheath solution.

To get an idea of the practical relevance of the different parameters controlling the presheath solution typical values for a SPT-100 type of Hall thruster are $\beta\sim 0.7$, $\tilde{T}_{iM}\ll 1$, $\nu_0 \sim 2-4\times 10^5\ \mathrm{s}^{-1}$, $\tilde{\nu}_i\sim 1$ in the ionization region and $\tilde{\nu}_i\ll 1$ outside it, and $\tilde{\nu}_r\sim 1$ in most of the channel.[13]

Finally, research is pursued in two directions. First, ceramic materials may present a secondary emission yield of order unity,[14,15] which is not immediate to include in a presheath/sheath model between two walls.[7] Second, a complete determination of the 2D conditions of the plasma discharge requires the simultaneous solving of the coupled radial and axial models.[13]

ACKNOWLEDGMENTS

This work was supported partially by the Dirección General de Enseñanza Superior e Investigación Científica of Spain, under Project No. PB97-0574-C04-02, and by the European Office for Aerospace Research and Development, under Contract No. F61775-01-WE070 (supervised by Dr. Ingrid Wysong).

APPENDIX A: DERIVATION OF THE RADIAL MODEL FROM THE AXISYMMETRIC MODEL

In a Hall thruster, ions are created by electron impact of a neutral gas, most of them are singly charged, and magnetic effects on them can be ignored. From the whole axisymmetric model, the equations relevant to study radial ion dynamics are

$$\frac{1}{r}\frac{\partial}{\partial r} r n_i v_{ri} + \frac{\partial}{\partial x}(n_i v_{xi}) = \nu_i n_i , \tag{A1}$$

$$m_i n_i \left(v_{ri}\frac{\partial v_{ri}}{\partial r} + v_{xi}\frac{\partial v_{ri}}{\partial x}\right) = -\frac{\partial}{\partial r}(n_i T_i) - e n_i \frac{\partial \phi}{\partial r} - \nu_i m_i n_i v_{ri} , \tag{A2}$$

$$\frac{1}{r}\frac{\partial}{\partial r}\left(r \frac{3}{2} T_i n_i v_{ri}\right) + \frac{\partial}{\partial x}\left(\frac{3}{2} T_i n_i v_{xi}\right) + T_i n_i \left(\frac{1}{r}\frac{\partial}{\partial r}(r v_{ri}) + \frac{\partial v_{xi}}{\partial x}\right) \tag{A3}$$

$$= \nu_i n_i \left(\tfrac{1}{2} m_i (v_{ri}^2 + v_{xi}^2) + \tfrac{3}{2} T_n\right). \tag{A4}$$

Here ν_i is the ionization frequency, T_n is the temperature of the neutral gas, and the rest of symbols are conventional. Ion heat conduction is not simple to estimate; here it has been disregarded, based in the conclusions of Scheuer and Emmert.[6] In Hall thrusters, T_n is negligible compared to the plasma temperature T_e; here, it is kept to compare our model with previous ones.

From the preceding equations, in each axial section of the chamber, ion radial dynamics verify

$$\frac{1}{r}\frac{\partial}{\partial r} r n_i v_{ri} = \nu_w n_i , \tag{A5}$$

$$m_i n_i v_{ri}\frac{\partial v_{ri}}{\partial r} = -\frac{\partial}{\partial r}(n_i T_i) - e n_i \frac{\partial \phi}{\partial r} - \nu_r m_i n_i v_{ri} , \tag{A6}$$

$$\frac{1}{r}\frac{\partial}{\partial r}\left(r \frac{3}{2} T_i n_i v_{ri}\right) + \frac{T_i n_i}{r}\frac{\partial}{\partial r}(r v_{ri}) = \nu_i \frac{1}{2} m_i n_i v_{ri}^2 + \nu_t n_i T_i , \tag{A7}$$

where axial dynamics are included through three frequency terms,

$$\nu_w \simeq \nu_i - \frac{1}{n_i}\frac{\partial}{\partial x}(n_i v_{xi}),$$

$$\nu_r \simeq \nu_i + \frac{v_{xi}}{v_{ri}}\frac{\partial v_{ri}}{\partial x}, \tag{A8}$$

$$\nu_t \simeq \frac{\nu_i}{T_i}\left(\frac{1}{2} m_i v_{xi}^2 + \frac{3}{2} T_n\right) - \frac{5}{2}\frac{\partial v_{xi}}{\partial x} - \frac{3 v_{xi}}{2 n_i T_i}\frac{\partial n_i T_i}{\partial x}.$$

These effective frequencies are unknown functions of x and r. The 1D radial model is based in taking $\nu_j = \nu_j(r)$, $(j=i,w,r,t)$, as known functions in a generic axial position x. [Effective frequencies for charge–exchange (ν_{cx}), electron–neutral (ν_{en}), and electron–ion (ν_{ei}) collisions have been omitted in Eq. (A2), based in the assumptions $\nu_{cx}\ll O(\nu_w)$ and $\nu_{en},\nu_{ei}\ll \nu_w m_i/m_e$, holding generally inside a Hall thruster. It would not be a problem to include them in the definition of ν_r.]

It is worth noting that the equations defining ν_w and ν_t in (A8), correspond also to the axial equations of continuity and energy for the average (i.e., r independent) plasma state,

$$\frac{\partial}{\partial x}(n_i v_{xi}) = (\nu_i - \nu_w) n_i , \tag{A9}$$

$$\frac{\partial}{\partial x}\left(\frac{3}{2}n_i T_i v_{xi}\right)+n_i T_i\frac{\partial v_{xi}}{\partial x}=\nu_i\left(\frac{1}{2}m_i n_i v_{xi}^2+\frac{3}{2}T_n\right)-\nu_t n_i T_i. \tag{A10}$$

Since the losses of internal energy at lateral walls per particle are $5T_i/2$, ν_t should be equal to $5\nu_w/2$, which coincides with the result found in Sec. II, Eq. (12), from the analysis of the radial energy equation.

In a Hall thruster, electrons diffuse axially in a quasi-closed drift induced by the radial magnetic field, whereas they remain confined radially by the self-induced electric potential. Therefore, we can assume that in the radial direction electrons are in Maxwell–Boltzmann equilibrium at a temperature T_e,

$$0\simeq -T_e\frac{\partial n_e}{\partial r}+en_e\frac{\partial\phi}{\partial r}. \tag{A11}$$

The Poisson equation for the axisymmetric problem is

$$\frac{\partial^2\phi}{\partial x^2}+\frac{1}{r}\frac{\partial}{\partial r}\left(r\frac{\partial\phi}{\partial r}\right)=\frac{e}{\epsilon_0}(n_e-n_i). \tag{A12}$$

Since the Debye length is much smaller than both the thruster dimensions and the relevant mean free paths, the zero Debye-length limit can be adopted to solve the problem. This means to consider the plasma quasineutral ($n_e\simeq n_i$) everywhere except in thin space-charge sheaths around the chamber walls, where a 1D form of Eq. (A12) can be used.

APPENDIX B: ON THE PRESHEATH/SHEATH TRANSITION

The quasineutral equations (1)–(5) show that it is impossible to have $|v_{ri}|>c_s$ in the presheath. But these equations by themselves do not forbid a presheath/sheath transition with $|v_{ri}|<c_s$, as Keidar *et al.*[10] propose. To settle that $|v_{ri}|=c_s$ is the only possible transition condition it is necessary to include the Poisson equation in the analysis.

Let us consider that the quasineutral solution extends until certain point Q with $v_{riQ}\leqslant c_{sQ}$ and $n_{eQ}=n_{iQ}$. The possibility of a transition to a non-neutral sheath depends on the local solution of the Poisson equation around point Q. Taking into account that the sheath is a thin region tied to the wall, radial gradients dominate within it and in the transition region, even for a plasma flowing axially. Then, the Poisson equation (A12) reduces there to the planar form

$$\frac{\epsilon_0}{e}\frac{\partial^2\phi}{\partial r^2}=n_e(\phi)-n_i(\phi,r), \tag{B1}$$

where the two density functions come from the plasma equations (1)–(5). Calling $\Delta\phi=\phi-\phi_Q$, $\Delta r=r-r_Q$, and $\lambda_{dQ}=\sqrt{\epsilon_0 T_e/e^2 n_{eQ}}$, the local expansion of Eq. (B1) around point Q is

$$\lambda_{dQ}^2\frac{\partial^2\Delta\phi}{\partial\Delta r^2}+a\Delta\phi+b\Delta\phi^2\simeq c\Delta r, \tag{B2}$$

with

$$a=\frac{T_e}{m_i v_{riQ}^2-\frac{5}{3}T_{iQ}}-1,\quad b=\frac{T_e}{2en_{iQ}}\left(\frac{\partial^2 n_i}{\partial\phi^2}-\frac{\partial^2 n_e}{\partial\phi^2}\right)\Bigg|_Q,$$
$$c=-\frac{T_e}{en_{iQ}}\frac{\partial n_i}{\partial r}\Bigg|_Q. \tag{B3}$$

Equation (B2) shows that for $a>0$, $\Delta\phi(\Delta r)$ can present only spatial oscillations around the quasineutral solution, $a\Delta\phi\simeq c\Delta r$. Therefore, a transition to a non-neutral sheath is possible only for $a\leqslant 0$.

For cold ions ($T_{iQ}=0$), $a\leqslant 0$ is equivalent to $v_{riQ}\geqslant c_{sQ}$. For warm ions, one has $a\leqslant 0$ for $v_{riQ}\geqslant c_{sQ}$ and for $v_{riQ}<\sqrt{5T_{iQ}/3m_i}$, but in this last case the sheath equations do not admit to have $v_{ri}>\sqrt{5T_{iQ}/3m_i}$ anywhere and wall conditions cannot be fulfilled [at least for $T_{iQ}/T_e\leqslant O(1)$]. Therefore, a transition to a sheath structure is only possible for $|v_{ri}|\geqslant c_s$. To conclude, since $v_{riQ}>c_{sQ}$ cannot be reached by the quasineutral solution, the sonic Bohm condition, $v_{ri}=c_{sQ}$ (i.e., $a=0$) is the *only possible* transition condition.

Once the transition point is uniquely determined, the solution of Eq. (B2) with $a=0$ yields the transition behavior of the electric potential and field. This problem was solved already by Tonks and Langmuir (see Fig. 6 in Ref. 1) and with some more detail and generality by Lam;[11] both works use kinetic models but the problem is solved in the same way for a macroscopic model. The solution of the transition region shows that (i) the electric field increases *continuously and smoothly* from $d\phi/dr\sim T_e/eh$ at the presheath side to $d\phi/dr\sim T_e/e\lambda_d$ at the sheath side and (ii)

$$\frac{d(e\phi/T_e)}{d\zeta}\Bigg|_Q=0 \tag{B4}$$

is the correct asymptotic boundary condition at the sheath edge in the sheath distinguished scale, $\zeta=(r-r_W)/\lambda_d$.

In the presence of a magnetic field oblique to the wall, another situation where Beilis and Keidar proposed a subsonic ion flow at the sheath edge,[16] Ref. 17 demonstrated that the sonic Bohm condition continues to give the correct presheath/sheath transition.

[1] L. Tonks and I. Langmuir, Phys. Rev. **34**, 876 (1929).
[2] D. Bohm, *The Characteristics of Electrical Discharges in Magnetic Fields* (MacGraw-Hill, New York, 1949), p. 77.
[3] E. Harrison and W. Thompson, Proc. Phys. Soc. London **74**, 145 (1959).
[4] G. Emmert, R. Wieland, A. Mense, and J. Davidson, Phys. Fluids **23**, 803 (1980).
[5] R. Bissell, P. Johnson, and P. Stangeby, Phys. Fluids B **1**, 1133 (1989).
[6] J. Scheuer and G. Emmert, Phys. Fluids B **2**, 445 (1990).
[7] E. Ahedo, P. Martínez-Cerezo, and M. Martínez-Sánchez, *37th Joint Propulsion Conference, Salt Lake City, UT* (American Institute of Aeronautics and Astronautics, Washington, DC, 2001), AIAA 2001-3323.
[8] J. Fife, M. Martínez-Sánchez, and J. Szabo, *33rd Joint Propulsion Conference, Seattle, WA* (American Institute of Aeronautics and Astronautics, Washington, DC, 1997), AIAA 97-3052.
[9] E. Ahedo and M. Martínez-Sánchez, *34th Joint Propulsion Conference, Cleveland, OH* (American Institute of Aeronautics and Astronautics, Washington, DC, 1998), AIAA 98-8788.
[10] M. Keidar, I. Boyd, and I. Beilis, Phys. Plasmas **8**, 5315 (2001).
[11] S. H. Lam, Phys. Fluids **8**, 73 (1965).
[12] E. Ahedo, P. Martínez-Cerezo, and M. Martínez-Sánchez, Phys. Plasmas **8**, 3058 (2001).

[13]E. Ahedo, P. Martínez-Cerezo, J. Gallardo, and M. Martínez-Sánchez, *27th International Electric Propulsion Conference, Pasadena, CA* (Electric Rocket Propulsion Society, Cleveland, OH, 2001), IEPC 01-17.
[14]J. Vaughan, IEEE Trans. Electron Devices **36**, 1963 (1989).
[15]L. Jolivet and J.-F. Roussel, *SP-465: 3rd Spacecraft Propulsion Conference, Cannes (France)* (European Space Agency, Noordwijk, The Netherlands, 2000), pp. 367–376.
[16]I. Beilis and M. Keidar, Phys. Plasmas **5**, 1545 (1998).
[17]E. Ahedo, Phys. Plasmas **4**, 4419 (1997); **6**, 4200 (1999).